

Supporting Information

An Ultra-thin, Un-doped NiO Hole Transporting Layer of Highly Efficient (16.4 %) Organic – Inorganic Hybrid Perovskite Solar Cells

Seongrok Seo,[†] Ik Jae Park,[†] Myungjun Kim, Seonhee Lee, Changdeuck Bae, Hyun Suk Jung, Nam-Gyu Park, Jin Young Kim,* and Hyunjung Shin*

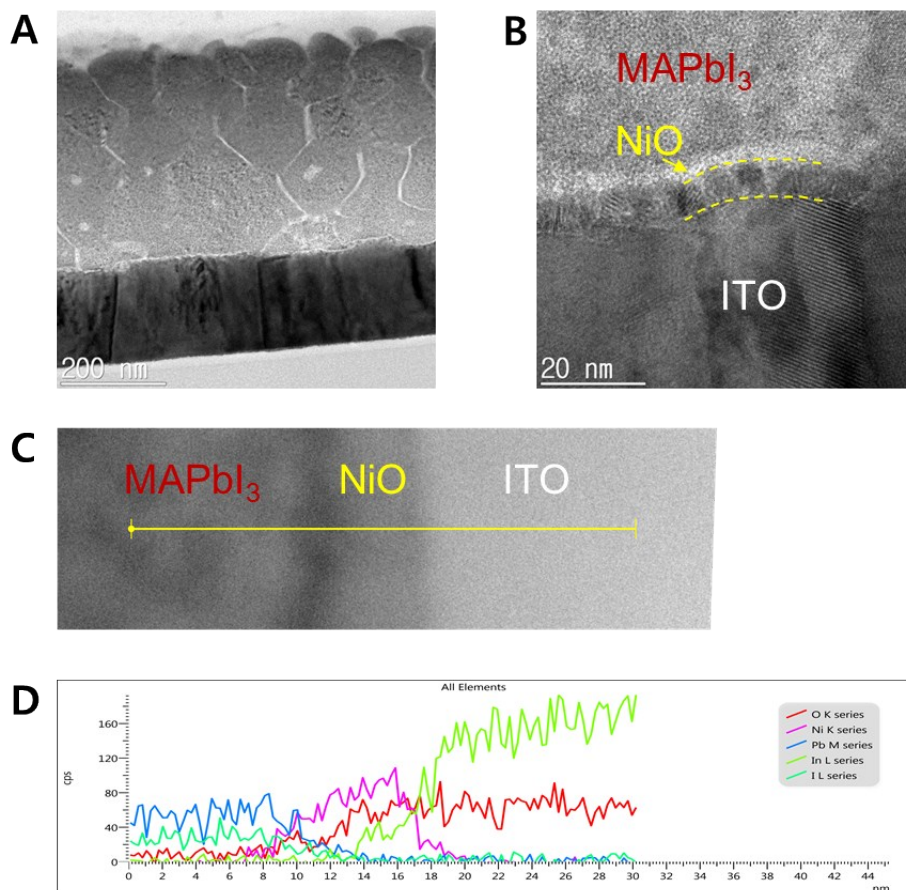


Figure S1. A) High-resolution bright field transmission electron microscopy image of the cross-sectional ITO/NiO/MAPbI₃ layer and B) is higher magnification of Fig. S1A). Thickness of 225 cycles of ALD-processed NiO onto ITO glass was determined to be 7 to 8 nm in Fig. S1B), which reveals the growth rate of NiO on ITO is similar to that of SiO₂/Si wafer. Figs. S1C) and D) show dark field scanning TEM image of cross-sectional ITO/NiO/MAPbI₃ and its line profile of energy dispersive X-ray (EDS).

The overall thickness of 225 cycles of ALD-processed NiO on ITO was determined to be 7 to 8 nm, which revealed the growth rate of NiO on ITO is similar to that of on SiO₂/Si wafer (0.34 nm/cycle). In any case, the TEM results (Figs. S1) proved “conformality” of ALD. ALD is a technique to deposit materials on arbitrary topography of surface in uniform of thickness without any line of sight. It can be done by sequential gas phase deposition with surface terminating chemical reactions. One of the reasons to change in growth behavior depending on different oxide substrates is the amount of hydroxyl group on the surface. Both of SiO₂/Si wafer and ITO glass were UV/Ozone treated before ALD process to make the sample being hydrophilic. Thus, it can be expected to have similar growth behavior in both substrates.

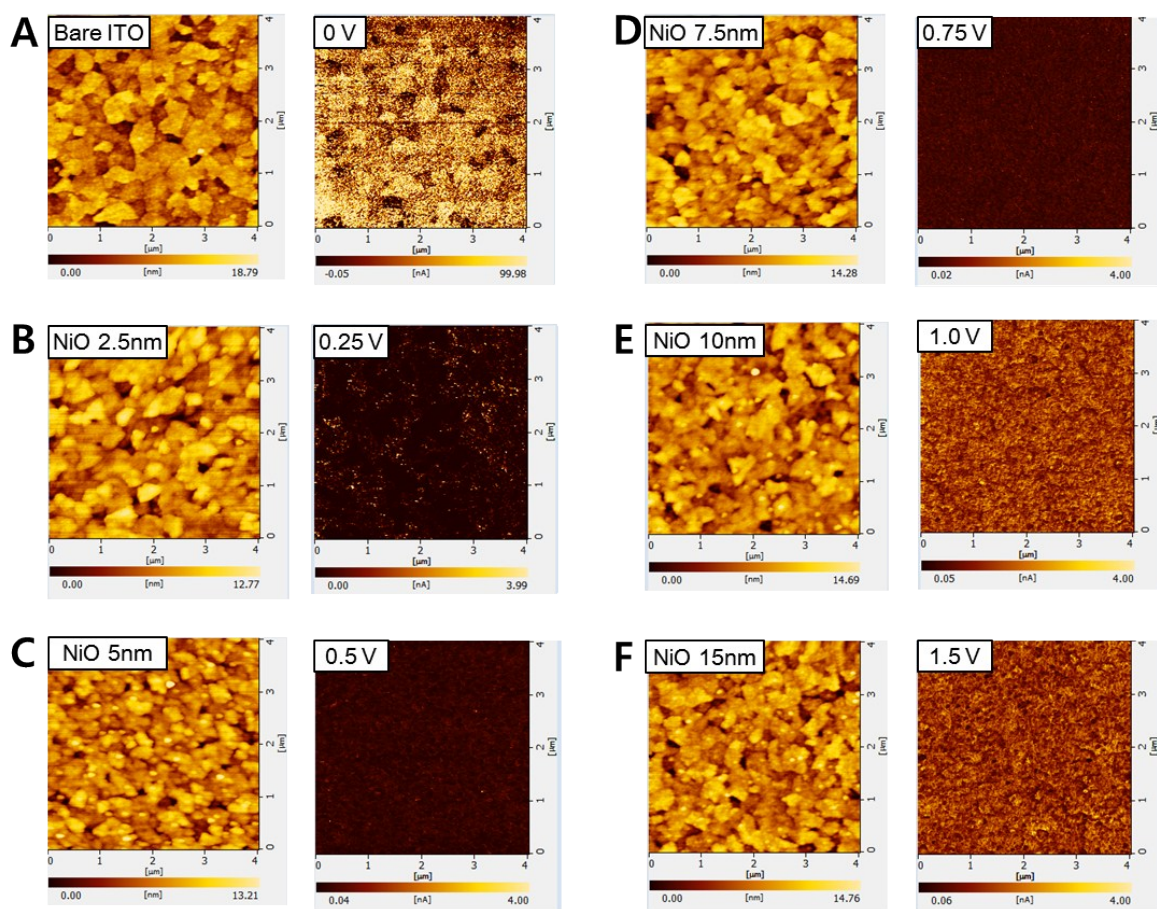


Figure S2. Thickness dependence of NiO (A-F) on morphology (left) and electrical property (right) measured by AFM and C-AFM, respectively. The surface roughness factor of RMS is about 2.95, 2.18, 2.08, 2.28, 2.23, and 2.27 nm for A-F. The comparison of current mapping was conducted at constant electric field of 1 MV/cm. There are not many differences between in RMS before and after NiO films' deposition. The result shows that the ALD-grown NiO films were uniformly coated on the ITO substrates structurally as well as electrically.

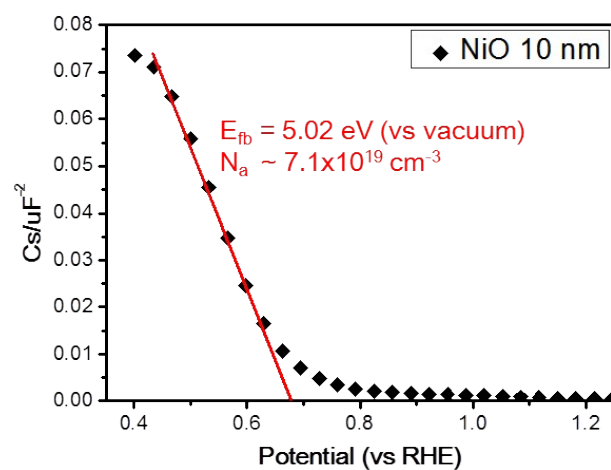


Figure S3. The detailed C^{-2} vs potential curve of NiO film (10 nm). The work function (flat band potential) and hole concentration were calculated by Mott-Schottky analysis. The decrease of C^{-2} from 0.4 to 0.8 potential (vs RHE) indicate the semiconducting type of our NiO is *p*-type.

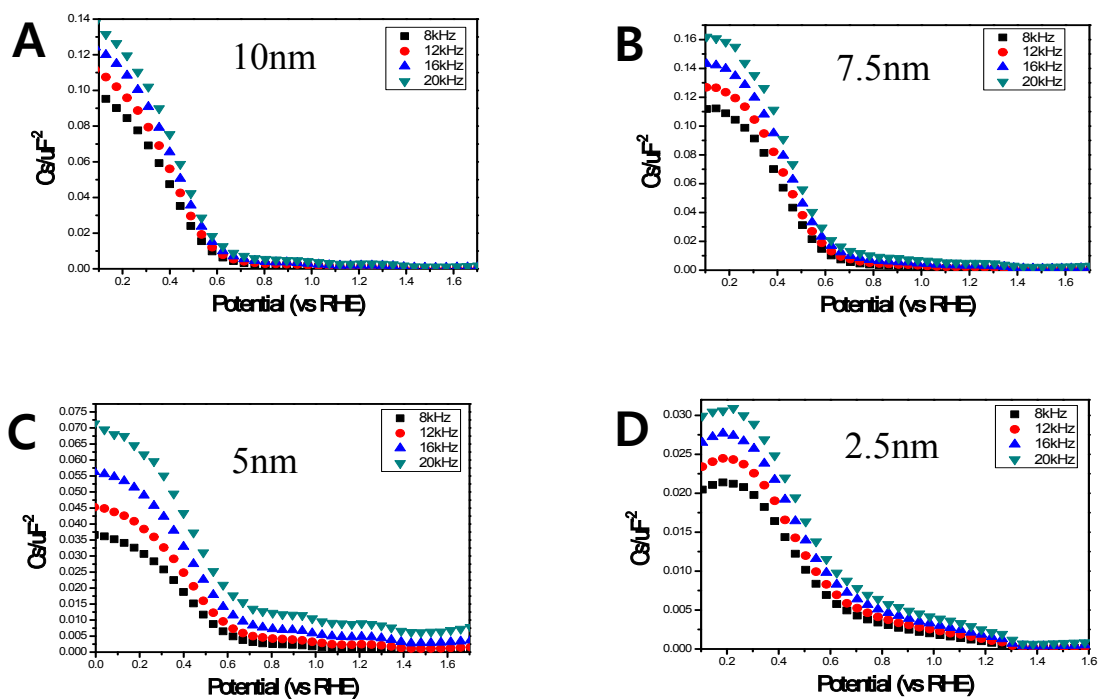


Figure S4: Electrochemical Mott-Schottky plots of NiO films with different thicknesses, 10 (A), 7.5 (B), 5 (C), and 2.5 nm (D) at selected frequencies (8, 12, 16, and 20 KHz) in pH = 11.96 electrolyte solution.

$$\Phi = h\nu - |E_{\text{cutoff}} - E_{\text{F}}| \quad \text{He I source : 21.22 eV}$$

NiO 10nm

$$\Phi = 21.22 - |17.11 - 0.82| = 4.93 \text{ eV}$$

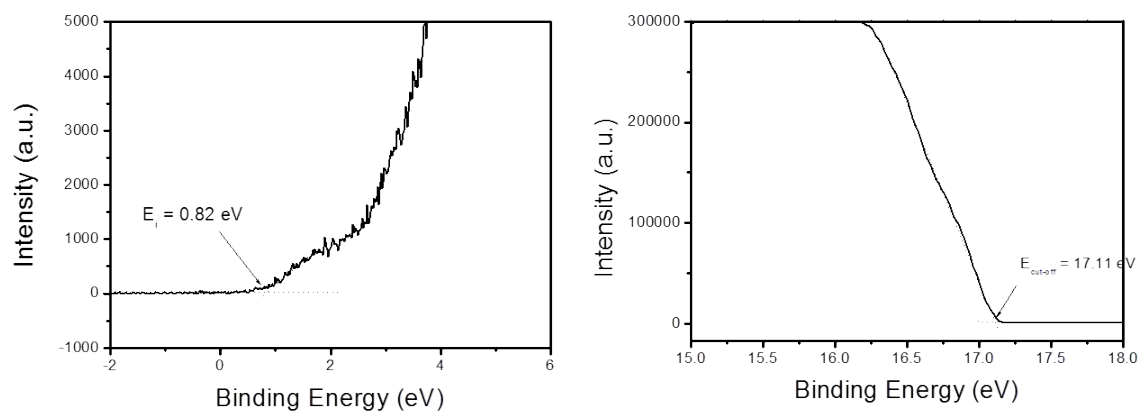


Figure S5. Ultraviolet photoelectron spectroscopy (UPS) spectra in the onset (E_i) and the cutoff (E_{cutoff}) energy regions of the surface measurement for the NiO on p^+ -Si film. The measured work function of NiO film was 4.93 eV.

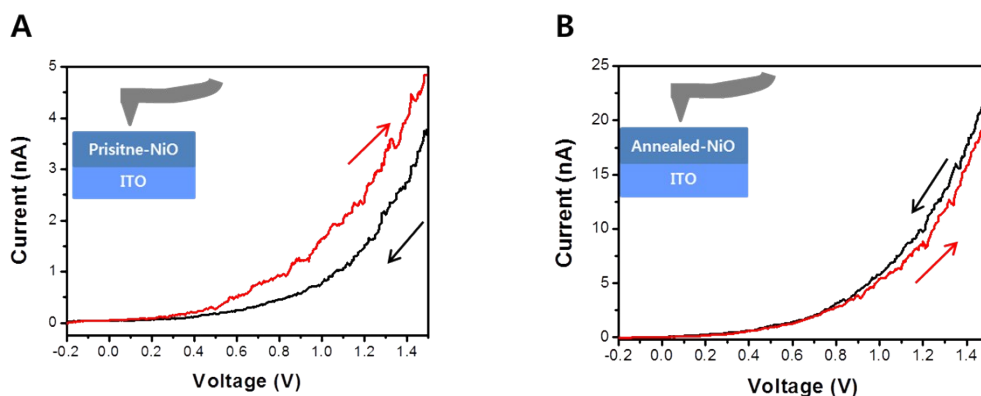


Figure S6. J - V characteristics under dark condition of ITO/NiO film with different scan directions (red line: forward, black line: reverse) measured by conductive atomic force microscopy (C-AFM) with different NiO film of A) Pristine NiO and B) Annealed NiO. Hysteresis was alleviated after annealing of NiO film.

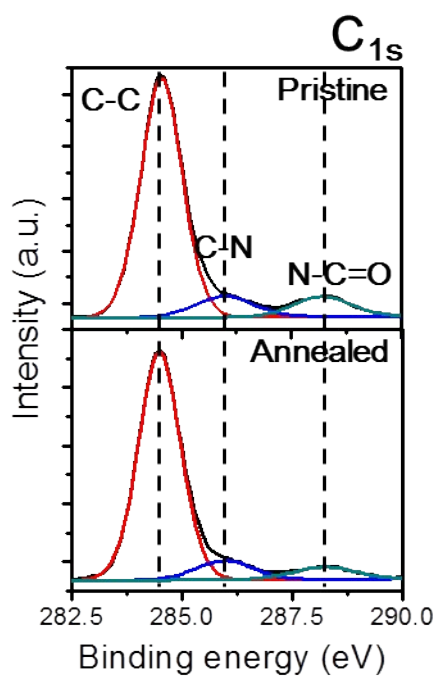


Figure S7. X-ray photoelectron spectroscopy of the NiO films with pristine (up) and annealed (down), respectively. XPS spectra at C 1s binding energies of NiO films were plotted.

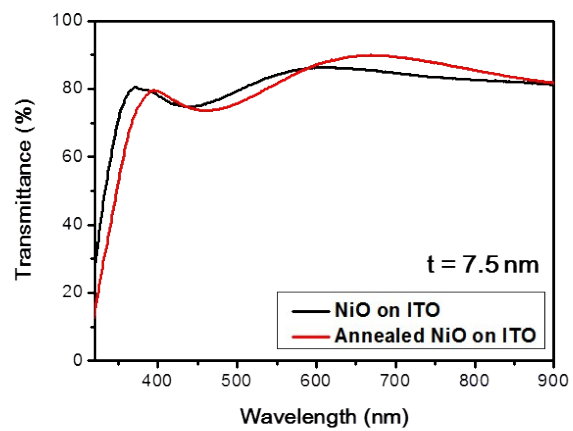


Figure S8. Optical transmission spectra of NiO films of ITO/pristine NiO (black line) and ITO/Annealed NiO (red line). The transmission spectrum of red line has red-shifted due to change of optical interference property of ITO/NiO film after annealing.